ACS Sustainable Chemistry & Engineering

Research Article

pubs.acs.org/journal/ascecg

An Efficient Way To Introduce Hierarchical Structure into Biomass-Based Hydrothermal Carbonaceous Materials

Yutong Gong, Haiyan Wang, Zhongzhe Wei, Lei Xie, and Yong Wang*

Carbon Nano Materials Group, ZJU-NHU United R&D Center, Center for Chemistry of High-Performance and Novel Materials, Key Lab of Applied Chemistry of Zhejiang Province, Department of Chemistry, Zhejiang University, 310028 Hangzhou, P. R. China

Supporting Information

ABSTRACT: Hydrothermal carbonization of biomass is regarded as the most sustainable technique to fabricate functional carbonaceous materials. The absence of nanoporous structures in the as-obtained materials remains a stumbling block to their wide applications. A hard-templating method and KOH activation are mostly frequently applied to introduce porous structures into HTC materials, but they always suffer from either tedious synthetic processes or massive use of a strong base. Here, the hierarchically porous structure was developed by heat treatment in the static air atmosphere. The textual properties were investigated by TEM and N_2 sorption analyses. The structural order and surface chemistry were characterized by XRD, Raman, and XPS. The results show that the activated HTC carbons are rich in micropores and mesopores with high surface areas up to 1704 m^2/g. The mesopore volume would reach over 50% of the total pore volume. In addition, these carbons show high performance in CO_2 and dye adsorption.

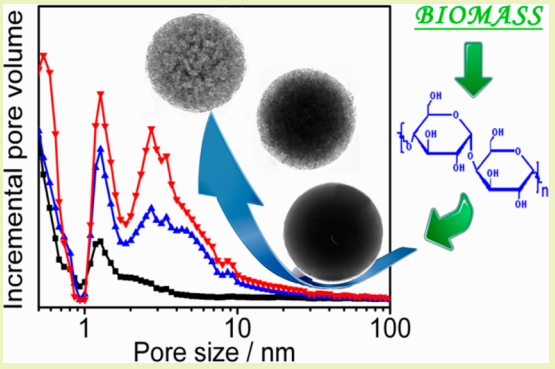

KEYWORDS: *Hydrothermal carbonization, Air activation, High mesopore ratio, Large surface area, CO_2 adsorption, Dye adsorption*

INTRODUCTION

Nanostructured carbon materials, especially those with high porosity, have attracted continuous attention due to their wide current and potential applications. They possess a variety of fascinating properties such as superior chemical and thermal stability, high surface areas, good conductivity, and tunable structures, by which they can be extended to the fields of adsorption,[1] sensing,[2] catalysis,[3] energy storage and conversion,[4] drug delivery,[5] separation science,[6] etc. In the past decades, various techniques have been explored for the production of carbons with different forms and morphologies. Bottom-up strategies such as electric arc discharge techniques,[7] catalytical chemical vapor deposition,[8] and catalytic pyrolysis of organic compounds[9] are frequently applied for the fabrication of carbon materials with specific nanostructures such as graphene, carbon nanotubes, and carbon spheres. Mass production is always high cost and causes pollution. The search for more sustainable and inexpensive synthetic strategies for the generation of carbon materials with controllable microstructures and nanostructures remains an appealing topic in materials chemistry.

Hydrothermal carbonization (HTC) of biomass in pure water has generated widespread interest throughout recent years and is even regarded as the most sustainable approach toward functional materials.[10−13] The precursors for this process are carbohydrates or carbohydrate-rich biomasses, which are renewable and highly abundant within the global biosphere.[11] The use of water as the reaction medium reduces pollution. The biomass-to-carbon conversion can proceed under relatively mild conditions (less than 300 °C).[10,14] Actually, the HTC process is not a new methodology. The history of the HTC process dates back to 1913 when Bergius described the hydrothermal transformation of cellulose into coal-like materials.[15] Recently, the need for exploring cheap and sustainable ways to access chemicals and carbons from raw materials other than crude oil or natural gas leads to the explosion of investigations in this field again. However, the carbonaceous materials collected directly after hydrothermal carbonization have the characteristic of possessing only a small number of micropores.[14] The absence of porosity limits its widespread use. Therefore, introducing porous structures into HTC materials arouses much attention. The combination of HTC with hard-template relying on the approaches invented by Ryoo et al.[16] is the most direct way to develop porous carbon materials. However, the massive use and tedious removal course of the hard template (for example, SiO_2) remains a stumbling block on its way to mass production. Besides, the micelle-mediated soft-templating strategies require sophisticated reaction conditions, either a too low substrate concentration or long reaction time.[17] The construction of carbogel by HTC is regarded as a fine approach to obtain carbon materials with relatively high surface areas, while the

Received: July 10, 2014
Revised: September 16, 2014
Published: September 17, 2014

drying step in supercritical CO_2 is always inevitable for structure preservation.[18,19]

Post-activation methods are widely applied to improve the textual properties for carbon materials, including HTC materials. The most frequently used activating reagents are strong bases (KOH, NaOH)[20,21] and acids (H_3PO_4).[22] Unfortunately, they still have some common drawbacks. First, equivalent or even multiple amounts of the activating agent to the HTC material will result in severe pollution. Second, although this activating strategy can generate high surface areas up to 2000−3000 m^2/g, the overwhelming majority of the developed pores are micropores,[20,23,24] which is unfavorable for mass transfer. In practice, the mesopores are more favorable in most technology important applications (e.g., heterogeneous catalysis, electrodes, sorption etc.) because the surface in the mesopores is more accessible for ions or molecules.

In most cases, post-carbonization at elevated temperatures is an essential step to increase structural order, material stability, and conductivity because the materials obtained directly from HTC can be seen as "organic" polymers,[25,26] which cannot resist mechanical force and high temperatures. The heat treatment process provides an ideal chance to activate the HTC materials. In this research, we present a facile way to produce hierarchically porous HTC carbons via activation by static air. In previous reports, air is applied as an activating reagent to modulate the surface chemistry instead of introduction of porous structures[27,28] because the carbon materials would completely decompose in higher temperatures up to 800 °C in flowing air. Here, we treated the HTC materials in a muffle oven vented to the atmosphere in the absence of inert gas. A surface area up to 1704 m^2/g with a high pore volume of 1.22 cm^3/g can be achieved. The mesopores account for more than 50% of the total pore volume. The porous structure can be introduced to the surface of the spherical carbonaceous spheres or even pass throughout them. It also proved to be a general method for HTC materials from carbohydrate (glucose, fructose, sucrose, starch, cellulose). These activated carbon materials showed promising adsorption capability for CO_2 and dyes.

EXPERIMENTAL DETAILS

All chemicals are purchased from Aladdin Chemical and are of analytical grade.

Preparation of the HTC Materials. Hydrothermal carbonaceous materials were prepared by a classical hydrothermal carbonization procedure.[29] In a typical process, a solution containing 4 g of glucose and 40 mL of water was sealed in a 50 mL Teflon-lined autoclave. The autoclave was put into a constant temperature oven of 180 °C and maintained for 4 h. Then, the brown or dark product was collected and washed several times with water and ethanol followed by drying at 80 °C in air. For other substrates (fructose, sucrose, starch, and cellulose), 8 g of carbohydrate was dissolved in 50 mL water and was hydrothermally treated in a 100 mL autoclave for 8 h. These materials were denoted as Glu-*x*, Fru-*x*, Suc-*x*, Sta-*x*, and Cel-*x*, where *x* represents the hydrothermal temperature.

Activation of HTC Materials. The dried HTC materials were activated at different temperatures (i.e., 600, 700, 800, 900 °C) in a muffle furnace connected to the outside atmosphere (Nabertherm L3/11, Gemary). Typically, 1g of dried HTC material was transferred into a crucible with a lid. Then, the temperature was elevated to the desired temperature in 1 h and was maintained for 1 h. The obtained black powders were marked as Glu-*x*-*y*, Fru-*x*-*y*, Suc-*x*-*y*, Sta-*x*-*y*, and Cel-*x*-*y* (*y* is the activating temperature).

Characterization. The morphologies were characterized by scanning electron microscopy (SEM, LEO 1550) and transmission electron microscopy (TEM, Hitachi H7700) with a CCD imaging system with an acceleration voltage of 100 kV. N_2 adsorption analysis was performed at 77 K using a Micromeritics ASAP 2020 to access the surface areas and pore size distributions. All the samples were outgassed at 200 °C for 12 h. Then adsorption−desorption processes were conducted between the relative pressure (P/P_0) range from 10^{-6} to 1. The specific surface area was calculated by the conventional Brunauere−Emmette−Teller (BET) method. The pore size distribution (PSD) plot was recorded by the DFT model. The micropore volume (V_{micro}) was estimated by using the *t*-plot method. The diffraction data were collected at room temperature with a 2θ scan range between 5° and 90° using wide-angle X-ray diffraction (Model D/tex-Ultima TV, 1.6 kV, Rig-aku, Japan) equipped with Cu Kα radiation (1.54 Å). The X-ray photoelectron spectra (XPS) information was accessed by an ESCALAB_250Xi instrument using a magnesium anode (Mg 1253.6 eV) X-ray source.

CO_2 Adsorption Experiment. The CO_2 adsorption was evaluated by the adsorption isotherms measured using a Micromeritics ASAP 2020 static volumetric analyzer at the setting temperature. Prior to each experiment, the sample was degassed for 6 h at 200 °C ensuring that the residual pressure fell below 5×10^{-3} mbar and then was cooled to the target temperature. Then, the gas adsorption capacity in terms of adsorbed volume under standard temperature and pressure (STP) was recorded.

Dye Adsorption Experiment. UV/vis spectrophotometry (Shimadzu, Japan) was applied to quantify the adsorption capacity of dyes. In a typical experimental run, 10 mg of Glu-180-900 was immerged into a dye solution with a known concentration. Then, the mixture was agitated with a magnetic stir. After equilibrium, the solutions were filtered with a Millipore filter, diluted, and measured with UV/vis spectrophotometry. The initial (C_0) and equilibrium concentrations (C_e) of the dyes are evaluated by Lambert−Beer's law. The adsorbed amounts (q) were calculated with the following equation

$$q = \frac{C_0 - C_e}{m} V$$

where V is the volume of the solution (L), and m is the mass of Glu-180-900 (g).

RESULTS AND DISCUSSION

For a better comparison of the activating degree of the HTC materials, we fabricated the monodispersed HTC-based carbon spheres, which can be controlled by the reaction conditions.[30] Figure 1 shows the SEM image of carbon spheres from the classical hydrothermal treatment of glucose at 180 °C. The carbon spheres are almost monodispersed, and the particle sizes range from 200 to 500 nm. All of the spheres are solid with a smooth surface.

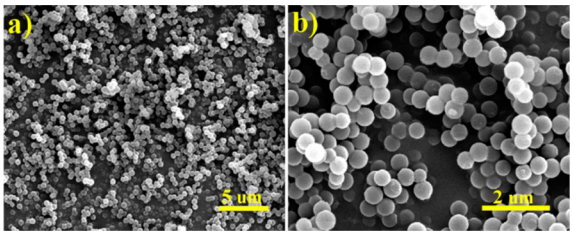

Figure 1. SEM images of the prepared Glu-180.

KOH is the frequently applied activating agent for HTC materials from carbohydrates.[21] For higher BET surface areas, the KOH amount used is two to four times of the HTC materials, which results in tedious removal processes and pollution problems.[20,31] To eliminate the usage of massive strong corrosive activating agents, air activation seems to be

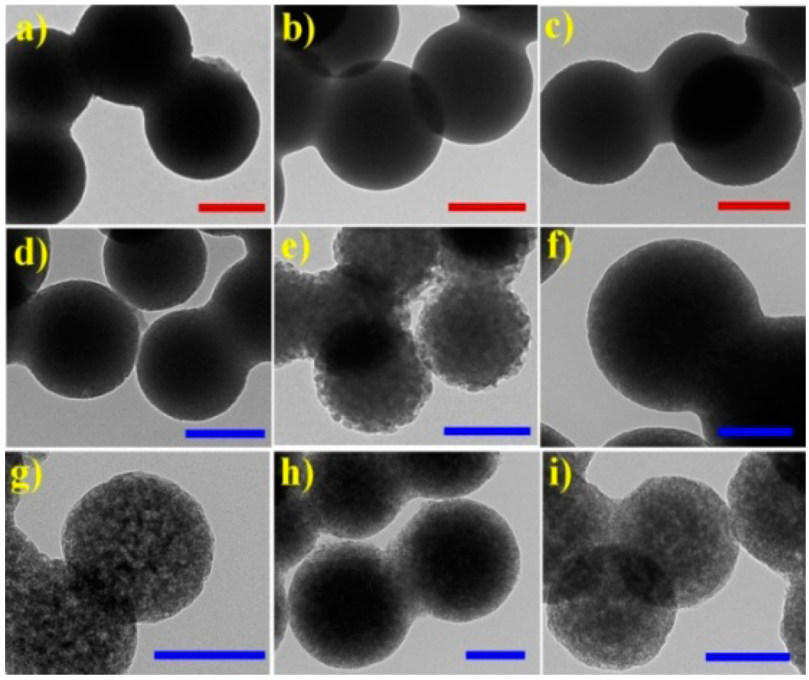

Figure 2. TEM images of Glu-180 (a), Glu-180-900N (b), Glu-180-600 (c),Glu-180-700 (d,e),Glu-180-800 (f,g), and Glu-180-900 (h,i). Red bar: 300 nm, Blue bar: 200 nm.

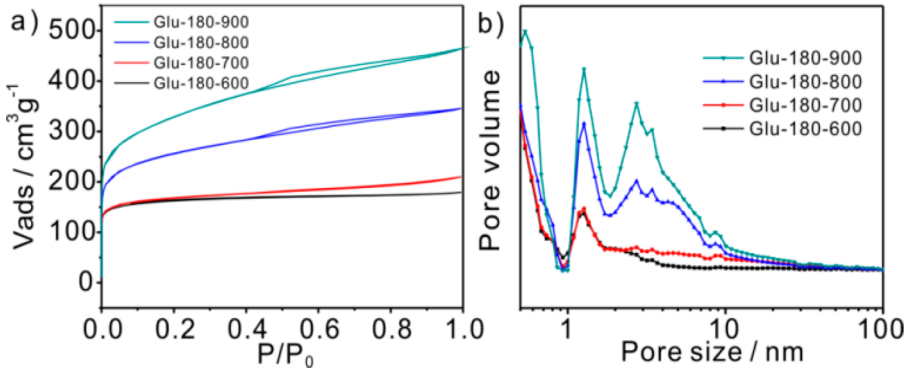

Figure 3. N_2 sorption isotherms (a) of Glu-180-600, Glu-180-700, Glu-180-800, Glu-180-900, and corresponding DFT pore size distributions (b).

perfect because carbonization and porosity can be gained at the same time without harmful byproducts. While in flowing air, the carbonaceous materials suffer from complete decomposition at high temperatures. For example, to activate glassy carbonaceous spheres made from resorcinol−formaldehyde, the temperature should be limited to under 450 °C with a long activating time (e.g., 72 h).[32] However, the developed porosity is mainly composed of micropores. Mesopores with sizes above 5 nm are negligibly small. Here, we designed the activation process in static air for HTC materials. The HTC carbonaceous materials were put into a crucible with a lid and calcined in a muffle oven connected with the outside atmosphere. The activation yield is comparable to that of a KOH activation process (Table S1, Supporting Information). Tuning the pore system by simply adjusting the activating temperature is an ideal option. In order to examine the influence of temperature on the porous structures, the employed temperature was varied over a range from 600 to 900 °C. TEM was applied to characterize the as-made Glu-180 and activated carbon materials. No porous structures can be observed in Glu-180 (Figure 2a), which is a common feature for all HTC materials from carbohydrates.[14] After heat treatment at 600 °C in air, visible rough edges can be viewed on the carbon spheres as shown in Figure 2c, although inconspicuous. When the activating temperature was raised to 700 °C, two obviously different morphologies can be seen in the TEM view. The first one possesses a pronounced pore-rich layer on the surface of the carbon spheres (Figure 2d). The other one is covered with multiple shallow flaws (Figure 2e), leading to a few mesopores and macropores. The conclusion was also drawn by the SEM images (Figure S1b, Supporting Information). The rough flaws on the surface result from the destruction of the unstable hydrophilic surface.[25,33] It is worth noting that the former morphology dominates Glu-180-700. The TEM images provide evidence that there is an abrupt morphological change above 800 °C. Obvious hierarchical pores are introduced into the bulk carbon. The pores either construct a distinct layer on the spheres or run through the entire sphere (Figure 2f−i). The surface flaws disappear due to the complete decomposition of the unstable layer. The porosity of Glu-180-900 is more pronounced than that of Glu-180-800. In contrast, no observed mesopores can be seen in the HTC materials calcined at 900

°C in N_2 atmosphere (Figure 2b). All the carbon spheres maintained their regular spherical shapes after activation.

N_2 adsorption−desorption isotherms were collected to quantify the textual properties, and the data were summarized in Figure 3 and Table 1. The BET surface area calculated for

Table 1. Textual Properties of Obtained Carbon Materials

entry	sample	S_{BET} ($m^2\ g^{-1}$)	V_{micro} ($cm^3\ g^{-1}$)	$V_{macro\&meso}$ ($cm^3\ g^{-1}$)	V_{total} ($cm^3\ g^{-1}$)
1	Glu-180	<5	–	–	0.01
2	Glu-180-600	557	0.256	0.004	0.26
3	Glu-180-700	577	0.24	0.08	0.32
4	Glu-180-800	893	0.33	0.20	0.53
5	Glu-180-900	1156	0.40	0.32	0.72
6	Glu-180-1000	1704	0.60	0.62	1.22
7	Fru-160-900	1043	0.31	0.28	0.59
8	Suc-180-900	1035	0.34	0.25	0.59
9	Sta-200-900	1041	0.36	0.25	0.61
10	Cel-230-900	1357	0.41	0.50	0.91

Glu-180 is very low (<5m^2/g), and no significant porosity is detected. As demonstrated in Figure 3a, Glu-180-600 shows a typical type-I isotherm according to the IUPAC classification. The isotherm displays a steep uptake of N_2 at low P/P_0 and arrived at an adsorptive saturation at ∼0.1 P/P_0 with no hysteresis over the whole range, indicating the characteristic for microporous materials. The corresponding pore size distribution on the basis of DFT calculations provide evidence that the pores are less than two nanometers in diameter. The BET surface area is 557 m^2/g with a pore volume of 0.26 cm^3/g. Compared to Glu-180-600, the sorption isotherm of Glu-180-700 shows a gentle slope between 0.2 and 1.0 P/P_0, which can be related to the existence of limited mesopores. The surface area increases to 577 m^2/g with a minor increase in pore volume to 0.32 $cm^3\ g^{-1}$. The isotherms of Glu-180-800 and Glu-180-900 combine type-I and type-IV with an obvious H1 hysteresis loop. The hysteresis loop demonstrates the presence of capillary condensation, reflecting the existence of considerable mesopores in the activated carbons. The steep uptake of N_2 at low P/P_0 suggests that the porous carbons also contain rich micropores. The coexistence of micropores and mesopores is consistent with the conclusion from TEM results and can also be supported by DFT pore size distributions. Upon the activating temperature being raised to 800 °C, mesopores ranging from 2 to 10 nm emerge (Figure 3b) and rise with the increasing temperature. Furthermore, both the surface areas and pore volumes are enhanced with an increase in temperature. A surface area up to 1156 m^2/g with a pore volume of 0.72 cm^3g^{-1} was achieved at 900 °C. What is more important to note is that the mesopore volume accounts for 44.4% of the total pore volume, exceeding that of the carbons activated by KOH. A 50.8% mesopore volume with a surface area of 1704 m^2/g can be gained via activation at 1000 °C, while the activation yield is relatively low (Table S1, Supporting Information). The micropores on the carbon particles can be interpreted by the reaction between the carbon atoms or fragments and oxygen as $C + O_2 \rightarrow CO$ and $C + O_2 \rightarrow CO_2$ in limited air atmosphere. The opening and cross-link of the micropores lead to formation of rich mesopores.

XRD analyses assisted in examining the structural order of the activated carbons. The as-prepared Glu-180 exhibits one

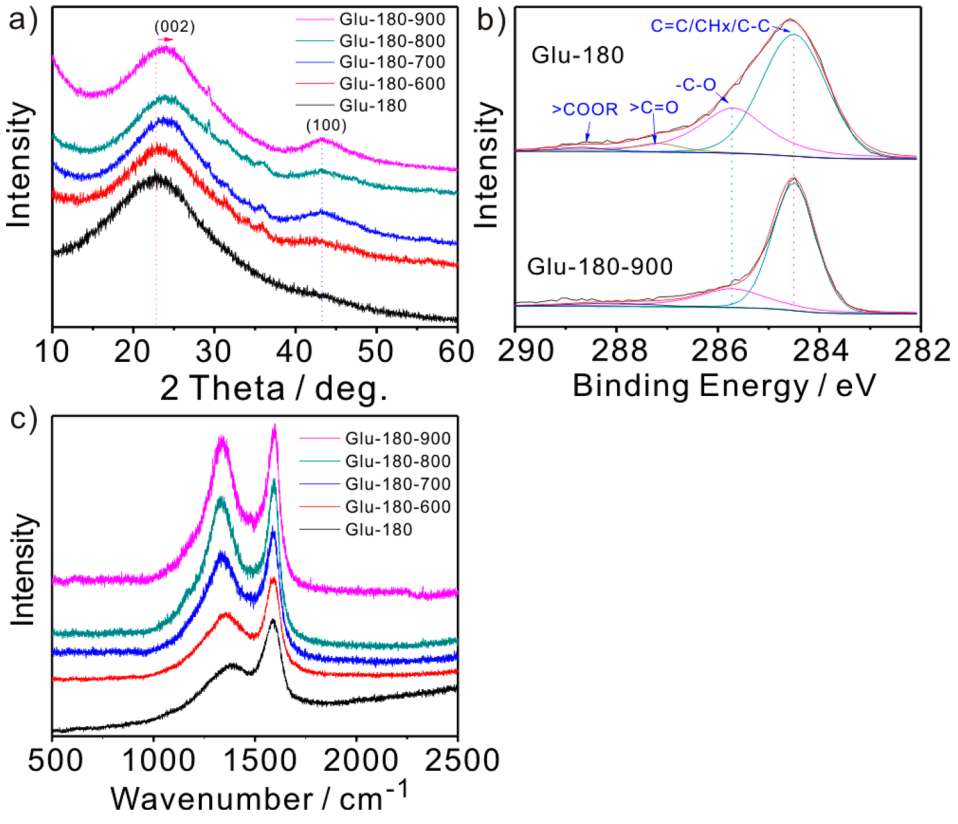

Figure 4. XRD analysis of Fru-180 and active carbons (a). C (1s) envelopes of Glu-180 and Glu-180-900 from XPS analysis (b). Raman spectra of Glu-180 and activated carbons (c).

broad peak at 22.7° attributed to 002 interlayer reflection among irregularly oriented polycyclic aromatic C sheets of amorphous carbon (Figure 4a). This peak shifts toward higher degrees after activation, implying a decrease in the interlayer spacing.[34] A new peak equivalent of the 100 in-plane scattering emerges at 43.3° and becomes more evident with increasing temperature, which is a symbol of an increasing degree of order in these materials.[35] Both the peaks are broad for the activated carbons, suggesting that they are also amorphous. XPS was also carried out to characterize the surface functionalities (e.g., OH groups). After activation at high temperature, the conclusion that the oxygen functional groups decrease can be drawn by the attenuation of the C−O bonding signals in the C (1s) envelopes (Figure 4b). The C_{1S} spectrum can be deconvoluted into four peaks corresponding to aromatic or alkyl aromatic groups (284.5 eV), phenolic groups or ethers (285.7 eV), carbonyl groups (287.2 eV), and carboxylic acid or lactone (288.6 eV). These four functional groups were generated from aromatization, dehydration, aldol condensation, and esterification, respectively, during the hydrothermal treatment process.[36,37]

The peak centered at 284.5 eV attributed to carbon groups (C═C, CH*x*, C−C) narrows down after calcination, demonstrating better carbonization. The carbonization of the HTC materials is also demonstrated by an increase in carbon content determined by elemental analysis (Table S2, Supporting Information). Two typical peaks for carbon materials are shown on the Raman spectra of the as-prepared carbon materials (Figure 4c). The peak at ∼1300 cm^{-1} is associated with vibrations of carbon atoms with dangling bonds, while the one at ∼1600 cm^{-1} corresponds to an E_{2g} mode of the graphite layer. The I_d/I_g values of the activated carbons are all larger than 0.5, indicating the amorphous carbon structure with a high content of lattice edges or defects in plane terminations of disordered graphite of carbon materials.[38]

The large surface area and pore volume are of high value in practical applications. CO_2 and dye adsorption were tested to verify the promising application of these porous HTC-based carbons. The capture and separation of CO_2 from the fuel exhaust of power plants has received much attention during the past decade due to the global warming issue. The abundant microporosity and mesoporosity provide sufficient access for CO_2 capture and storage. Glu-180-900 was taken as the representative to investigate the CO_2 capacity at 0 and 25 °C. The analysis of the CO_2 adsorption isotherms is presented in Figure 5. At 0 °C and 780 mmHg, the maximum CO_2 uptake can reach 4.02 mmol/g, which was much higher than pristine Glu-180 (Figure S2, Supporting Information). When the measurement was carried out at 25 °C, it showed an adsorption capacity of 2.72 mmol/g. The value is higher than the widely applied actived carbons (<2 mmol/g)[39] and mesoporous carbons fabricated by a soft template (2.39 mmol/g)[40] and hard template (CMK-3, 1.7 mmol/g).[41] It is even comparable or superior to some MOFs and aminated HTC materials.[42−45] The Glu-180-900 also demonstrates high selectivity for CO_2 over N_2. For example, the N_2 uptake is just 0.30 mmol/g at 25 °C and 780 mmHg. The initial slopes of the CO_2 and N_2 adsorption isotherms were calculated, and the ratios of these slopes were used to estimate the adsorption selectivity for CO_2 over N_2. The CO_2/N_2 selectivity is calculated to be 22.0, indicating that Glu-180-900 has high selectivity for CO_2 (Figure S3, Supporting Information).[41] In addition, these air-activated HTC materials have great potential for improvement by introduction of functional groups such as the amino groups.

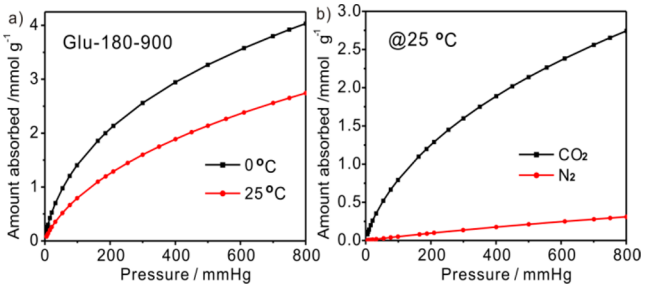

Figure 5. CO_2 adsorption isotherms of Glu-180-900 at different temperatures (a). CO_2 and N_2 adsorption isotherms of Glu-180-900 at 25 °C (b).

The effluents from industries such as textiles, paper, rubber, plastics, and cosmetics processes contain portions of dyes, which are deeply colored, multicomponent, and have low biodegradability, have become some of the most serious pollutants in water.[46] Tremendous efforts have been devoted to search for solutions, among which adsorption by porous carbon materials is one of the most efficient processes for dye removal and decoloration.[47,48] The adsorption performance of Glu-180-900 was investigated for six dyes. As displayed in Figure 6a,

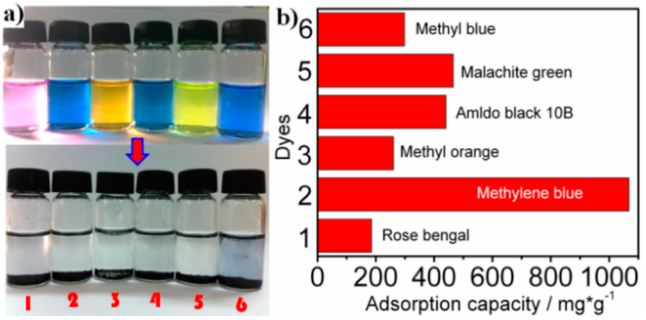

Figure 6. Optical photographs for dye-polluted water before and after adsorption by Glu-40-900 (a). Equilibrium absorption capacity of corresponding dyes (b).

almost all the dye solutions can be bleached, demonstrating a promising adsorption capability of Glu-180-900 for dyes. The saturated adsorption capacities were further measured by UV−vis spectrophotometry, and the results were displayed in Figure 6b. Glu-180-900 shows an outstanding adsorption capacity of 1068 mg/g, which is much improved over unactivated Glu-180 (177 mg/g) and is higher than that of commercial active carbon, some natural materials, and miscellaneous materials, etc.[49] It shows general efficiency for rose bengal (185 mg/g), methyl orange (260 mg/g), amldo black 10B (440 mg/g), malachite green (465 mg/g), and methyl blue (298 mg/g) as well, revealing a bright prospect for water purification.

To examine the generality of this methodology, different carbohydrate-based (fructose, sucrose, starch, cellulose) HTC materials were activated by the same method. The hierarchical structures were developed in Fru-160-900, Suc-180-900, Sta-200-900, and Cel-230-900, which are demonstrated by TEM and N_2 sorption analysis. The as-prepared Fru-160 and Cel-230 are irregular in shape. The hierarchically porous structures run through these relatively small carbonaceous particles after being activated in air at 900 °C (Figure 7a, d). Suc-180-900 and Sta-

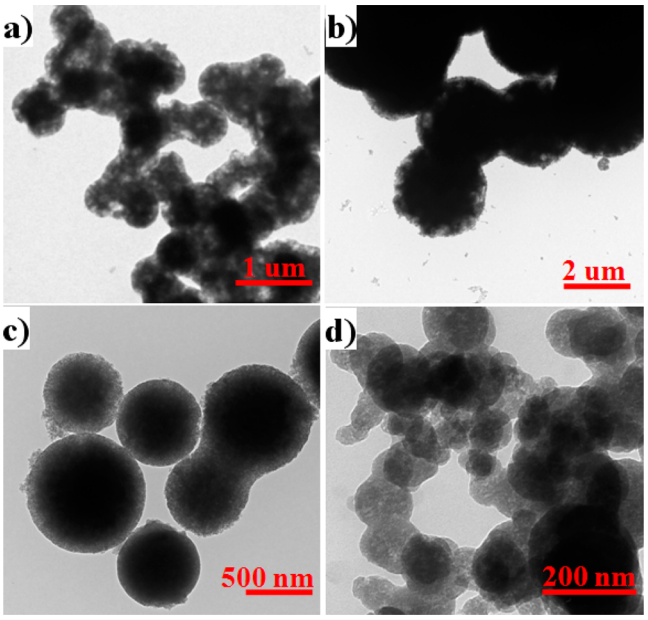

Figure 7. TEM images of Fru-160-900, Suc-180-900, Sta-200-900, and Cel-230-900.

230-900 are dominated by irregular carbon spheres larger than 500 nm, and the porous structures mainly exist in the surface of the spheres (Figure 7b, c). The result of N_2 sorption analysis shows that the BET surface areas are all over 1000 m^2/g. For Cel-230-900, the BET surface area reaches as large as 1357 m^2/g. The desired mesopores comprised a full 54.9% of the total pore volume (Table 1, entry 10). The value is seldom attained by strong bases. CO_2 uptake over 4.0 mmol/g and 2.5 mmol/g were achieved at 0 and 25 °C for all the activated HTC carbons at 780 mmHg (Figure S4, Supporting Information). These results indicate that the activating technique by air is a general method to introduce hierarchically porous structures into carbohydrate-based HTC materials.

CONCLUSIONS

In summary, we activated the nonporous biomass-based HTC materials to hierarchical carbons with a high surface area and considerable amount of mesopores. The method is generally effective for HTC materials from both monosaccharide and polysaccharide. It eliminates the massive use of harsh-activating reagents such as H_3PO_4 or KOH and provides a facile way for the production of biomass-based hierarchically porous carbon materials. The air-activated carbons by this method are effective in CO_2 and dye adsorption.

ASSOCIATED CONTENT

Supporting Information

Carbon yield, elemental analysis, SEM images, and CO_2 adsorption isotherms. This material is available free of charge via the Internet at http://pubs.acs.org.

AUTHOR INFORMATION

Corresponding Author

*E-mail: chemwy@zju.edu.cn.

Notes

The authors declare no competing financial interest.

ACKNOWLEDGMENTS

Financial support from the National Natural Science Foundation of China (21376208 and U1162124), Zhejiang Provincial Natural Science Foundation for Distinguished Young Scholars of China (R13B030002), Specialized Research Fund for the Doctoral Program of Higher Education (J20130060), Fundamental Research Funds for the Central Universities, Program for Zhejiang Leading Team of S&T Innovation, and Partner Group Program of the Zhejiang University and Max Planck Society are greatly appreciated.

REFERENCES

(1) Bae, Y. S.; Snurr, R. Q. Development and evaluation of porous materials for carbon dioxide separation and capture. *Angew. Chem., Int. Ed.* **2011**, *50* (49), 11586−11596.
(2) Melde, B. J.; Johnson, B. J. Mesoporous materials in sensing: Morphology and functionality at the meso-interface. *Anal. Bioanal. Chem.* **2010**, *398* (4), 1565−1573.
(3) Zhang, P. F.; Gong, Y. T.; Li, H. R.; Chen, Z. R.; Wang, Y. Solvent-free aerobic oxidation of hydrocarbons and alcohols with Pd@N-doped carbon from glucose. *Nat. Commun.* **2013**, *4*, 1593.
(4) Dai, L. M.; Chang, D. W.; Baek, J. B.; Lu, W. Carbon nanomaterials for advanced energy conversion and storage. *Small* **2012**, *8* (8), 1130−1166.
(5) Yamashita, T.; Yamashita, K.; Nabeshi, H.; Yoshikawa, T.; Yoshioka, Y.; Tsunoda, S.; Tsutsumi, Y. Carbon nanomaterials: Efficacy and safety for nanomedicine. *Materials* **2012**, *5* (2), 350−363.
(6) Leboda, R.; Lodyga, A.; Gierak, A. Carbon adsorbents as materials for chromatography 0.1. Gas chromatography. *Mater. Chem. Phys.* **1997**, *51* (3), 216−232.
(7) Thess, A.; Lee, R.; Nikolaev, P.; Dai, H. J.; Petit, P.; Robert, J.; Xu, C. H.; Lee, Y. H.; Kim, S. G.; Rinzler, A. G.; Colbert, D. T.; Scuseria, G. E.; Tomanek, D.; Fischer, J. E.; Smalley, R. E. Crystalline ropes of metallic carbon nanotubes. *Science* **1996**, *273* (5274), 483−487.
(8) Eftekhari, A.; Jafarkhani, P.; Moztarzadeh, F. High-yield synthesis of carbon nanotubes using a water-soluble catalyst support in catalytic chemical vapor deposition. *Carbon* **2006**, *44* (7), 1343−1345.
(9) Gherghel, L.; Kübel, C.; Lieser, G.; Räder, H.-J.; Müllen, K. Pyrolysis in the mesophase: A chemist's approach toward preparing carbon nano- and microparticles. *J. Am. Chem. Soc.* **2002**, *124* (44), 13130−13138.
(10) Hu, B.; Wang, K.; Wu, L. H.; Yu, S. H.; Antonietti, M.; Titirici, M. M. Engineering carbon materials from the hydrothermal carbonization process of biomass. *Adv. Mater.* **2010**, *22* (7), 813−828.
(11) Yu, L. H.; Falco, C.; Weber, J.; White, R. J.; Howe, J. Y.; Titirici, M. M. Carbohydrate-derived hydrothermal carbons: A thorough characterization study. *Langmuir* **2012**, *28* (33), 12373−12383.
(12) Hu, B.; Yu, S.-H.; Wang, K.; Liu, L.; Xu, X.-W. Functional carbonaceous materials from hydrothermal carbonization of biomass: an effective chemical process. *Dalton. Trans.* **2008**, *40*, 5414−5423.
(13) Gong, Y.; Xie, L.; Li, H.; Wang, Y. Sustainable and scalable production of monodisperse and highly uniform colloidal carbonaceous spheres using sodium polyacrylate as the dispersant. *Chem. Commun.* **2014**, DOI: 10.1039/C4CC04998E.
(14) Titirici, M. M.; Antonietti, M. Chemistry and materials options of sustainable carbon materials made by hydrothermal carbonization. *Chem. Soc. Rev.* **2010**, *39* (1), 103−116.
(15) Bergius, F. Die Anwendung hoher Drücke bei chemischen Vorgängen und eine Nachbildung des Entstehungsprozesses der Steinkohle. *Z. Elektrochem. Angew. Phys. Chem.* **1913**, *20*, 260.
(16) Ryoo, R.; Joo, S. H.; Jun, S. Synthesis of highly ordered carbon molecular sieves via template-mediated structural transformation. *J. Phys. Chem. B* **1999**, *103* (37), 7743−7746.
(17) Kubo, S.; White, R. J.; Yoshizawa, N.; Antonietti, M.; Titirici, M. M. Ordered carbohydrate-derived porous carbons. *Chem. Mater.* **2011**, *23* (22), 4882−4885.

(18) White, R. J.; Yoshizawa, N.; Antonietti, M.; Titirici, M. M. A sustainable synthesis of nitrogen-doped carbon aerogels. *Green Chem.* **2011**, *13* (9), 2428−2434.
(19) Fellinger, T. P.; White, R. J.; Titirici, M. M.; Antonietti, M. Borax-mediated formation of carbon aerogels from glucose. *Adv. Funct. Mater.* **2012**, *22* (15), 3254−3260.
(20) Sevilla, M.; Fuertes, A. B. Sustainable porous carbons with a superior performance for CO_2 capture. *Energy Environ. Sci.* **2011**, *4* (5), 1765−1771.
(21) Falco, C.; Marco-Lozar, J. P.; Salinas-Torres, D.; Morallon, E.; Cazorla-Amoros, D.; Titirici, M. M.; Lozano-Castello, D. Tailoring the porosity of chemically activated hydrothermal carbons: Influence of the precursor and hydrothermal carbonization temperature. *Carbon* **2013**, *62*, 346−355.
(22) Romero-Anaya, A. J.; Lillo-Rodenas, M. A.; de Lecea, C. S. M.; Linares-Solano, A. Hydrothermal and conventional H_3PO_4 activation of two natural bio-fibers. *Carbon* **2012**, *50* (9), 3158−3169.
(23) Zhao, L.; Fan, L. Z.; Zhou, M. Q.; Guan, H.; Qiao, S. Y.; Antonietti, M.; Titirici, M. M. Nitrogen-containing hydrothermal carbons with superior performance in supercapacitors. *Adv. Mater.* **2010**, *22* (45), 5202−+.
(24) Wei, L.; Sevilla, M.; Fuertes, A. B.; Mokaya, R.; Yushin, G. Hydrothermal carbonization of abundant renewable natural organic chemicals for high-performance supercapacitor electrodes. *Adv. Energy Mater.* **2011**, *1* (3), 356−361.
(25) Sevilla, M.; Fuertes, A. B. The production of carbon materials by hydrothermal carbonization of cellulose. *Carbon* **2009**, *47* (9), 2281−2289.
(26) Falco, C.; Caballero, F. P.; Babonneau, F.; Gervais, C.; Laurent, G.; Titirici, M. M.; Baccile, N. Hydrothermal carbon from biomass: Structural differences between hydrothermal and pyrolyzed carbons via C-13 solid state NMR. *Langmuir* **2011**, *27* (23), 14460−14471.
(27) Roman, S.; Nabais, J. M. V.; Ledesma, B.; Gonzalez, J. F.; Laginhas, C.; Titirici, M. M. Production of low-cost adsorbents with tunable surface chemistry by conjunction of hydrothermal carbonization and activation processes. *Microporous Mesoporous Mater.* **2013**, *165*, 127−133.
(28) Chen, Z.; Ma, L. J.; Li, S. Q.; Geng, J. X.; Song, Q.; Liu, J.; Wang, C. L.; Wang, H.; Li, J.; Qin, Z.; Li, S. J. Simple approach to carboxyl-rich materials through low-temperature heat treatment of hydrothermal carbon in air. *Appl. Surf. Sci.* **2011**, *257* (20), 8686−8691.
(29) Sun, X. M.; Li, Y. D. Colloidal carbon spheres and their core/shell structures with noble-metal nanoparticles. *Angew. Chem., Int. Ed.* **2004**, *43* (5), 597−601.
(30) Li, M.; Li, W.; Liu, S. X. Control of the morphology and chemical properties of carbon spheres prepared from glucose by a hydrothermal method. *J. Mater. Res.* **2012**, *27* (8), 1117−1123.
(31) Li, M.; Li, W.; Liu, S. X. Hydrothermal synthesis, characterization, and KOH activation of carbon spheres from glucose. *Carbohyd. Res.* **2011**, *346* (8), 999−1004.
(32) Inagaki, M.; Park, C. R.; Skowronski, J. M.; Morawski, A. W. Glass-like carbon spheres − Activation, porosity and application possibilities. *Adsorpt. Sci. Technol.* **2008**, *26* (10), 735−787.
(33) Sun, X.; Li, Y. Colloidal carbon spheres and their core/shell structures with noble-metal nanoparticles. *Angew. Chem., Int. Ed.* **2004**, *43* (5), 597−601.
(34) Jin, Y. Z.; Kim, Y. J.; Gao, C.; Zhu, Y. Q.; Huczko, A.; Endo, M.; Kroto, H. W. High temperature annealing effects on carbon spheres and their applications as anode materials in Li-ion secondary battery. *Carbon* **2006**, *44* (4), 724−729.
(35) Zhao, L.; Baccile, N.; Gross, S.; Zhang, Y. J.; Wei, W.; Sun, Y. H.; Antonietti, M.; Titirici, M. M. Sustainable nitrogen-doped carbonaceous materials from biomass derivatives. *Carbon* **2010**, *48* (13), 3778−3787.
(36) Sevilla, M.; Fuertes, A. B. Chemical and structural properties of carbonaceous products obtained by hydrothermal carbonization of saccharides. *Chem.—Eur. J.* **2009**, *15* (16), 4195−4203.
(37) Kubo, S.; Tan, I.; White, R. J.; Antonietti, M.; Titirici, M. M. Template synthesis of carbonaceous tubular nanostructures with tunable surface properties. *Chem. Mater.* **2010**, *22* (24), 6590−6597.
(38) Mi, Y. Z.; Hu, W. B.; Dan, Y. M.; Liu, Y. L. Synthesis of carbon micro-spheres by a glucose hydrothermal method. *Mater. Lett.* **2008**, *62* (8−9), 1194−1196.
(39) Himeno, S.; Komatsu, T.; Fujita, S. High-pressure adsorption equilibria of methane and carbon dioxide on several activated carbons. *J. Chem. Eng. Data* **2005**, *50* (2), 369−376.
(40) Saha, D.; Deng, S. G. Adsorption equilibrium and kinetics of CO_2, CH_4, N_2O, and NH_3 on ordered mesoporous carbon. *J. Colloid Interface Sci.* **2010**, *345* (2), 402−409.
(41) Hao, G.-P.; Li, W.-C.; Qian, D.; Wang, G.-H.; Zhang, W.-P.; Zhang, T.; Wang, A.-Q.; Schüth, F.; Bongard, H.-J.; Lu, A.-H. Structurally designed synthesis of mechanically stable poly(benzoxazine-co-resol)-based porous carbon monoliths and their application as high-performance CO_2 capture sorbents. *J. Am. Chem. Soc.* **2011**, *133* (29), 11378−11388.
(42) Banerjee, R.; Furukawa, H.; Britt, D.; Knobler, C.; O'Keeffe, M.; Yaghi, O. M. Control of pore size and functionality in isoreticular zeolitic imidazolate frameworks and their carbon dioxide selective capture properties. *J. Am. Chem. Soc.* **2009**, *131* (11), 3875−3877.
(43) Wang, B.; Cote, A. P.; Furukawa, H.; O'Keeffe, M.; Yaghi, O. M. Colossal cages in zeolitic imidazolate frameworks as selective carbon dioxide reservoirs. *Nature* **2008**, *453* (7192), 207−212.
(44) An, J.; Geib, S. J.; Rosi, N. L. High and selective CO_2 uptake in a cobalt adeninate metal−organic framework exhibiting pyrimidine- and amino-decorated pores. *J. Am. Chem. Soc.* **2009**, *132* (1), 38−39.
(45) Zhao, L.; Bacsik, Z.; Hedin, N.; Wei, W.; Sun, Y. H.; Antonietti, M.; Titirici, M. M. Carbon Dioxide capture on amine-rich carbonaceous materials derived from glucose. *ChemSusChem* **2010**, *3* (7), 840−845.
(46) Zhuang, X.; Wan, Y.; Feng, C. M.; Shen, Y.; Zhao, D. Y. Highly efficient adsorption of bulky dye molecules in wastewater on ordered mesoporous carbons. *Chem. Mater.* **2009**, *21* (4), 706−716.
(47) Tanthapanichakoon, W.; Ariyadejwanich, P.; Japthong, P.; Nakagawa, K.; Mukai, S. R.; Tamon, H. Adsorption-desorption characteristics of phenol and reactive dyes from aqueous solution on mesoporous activated carbon prepared from waste tires. *Water Res.* **2005**, *39* (7), 1347−1353.
(48) Tamai, H.; Yoshida, T.; Sasaki, M.; Yasuda, H. Dye adsorption on mesoporous activated carbon fiber obtained from pitch containing yttrium complex. *Carbon* **1999**, *37* (6), 983−989.
(49) Rafatullah, M.; Sulaiman, O.; Hashim, R.; Ahmad, A. Adsorption of methylene blue on low-cost adsorbents: A review. *J. Hazard. Mater.* **2010**, *177* (1−3), 70−80.